NOx emissions by real-world fresh and old asphalt mixtures: Impact of temperature, relative humidity, and UV-irradiation

J. Lasne, A. Lostier, T. Salameh, E. Athanasopoulou, D. Karagiannis, A. Kakouri, S. Vassaux, D. Lesueur, M.N. Romanias

NOx Emissions by Real-World Fresh and Old Asphalt Mixtures: Impact of Temperature, Relative Humidity, and UV-Irradiation

J. Lasne[1,+,*], A. Lostier[1], T. Salameh[1], E. Athanasopoulou[2], D. Karagiannis[2], A. Kakouri[2], S. Vassaux[3], D. Lesueur[3], M.N. Romanias[1,*]

[1] IMT Nord Europe, Institut Mines-Télécom, Univ. Lille, Centre for Energy and Environment, F-59000 Lille, France
[2] Institute for Environmental Research and Sustainable Development, National Observatory of Athens, 15236 Athens, Greece
[3] IMT Nord Europe, Institut Mines-Télécom, Univ. Lille, Centre for Materials and Processes, F-59000 Lille, France

[+] Now also at: Laboratoire des Technologies Innovantes, UR 3899 - Université de Picardie Jules Verne, IUT Amiens, Avenue des Facultés, Le Bailly, CEDEX 1, 80025 Amiens, France
* Corresponding authors: jerome.lasne@imt-nord-europe.fr; emmanouil.romanias@imt-nord-europe.fr

Graphical Abstract

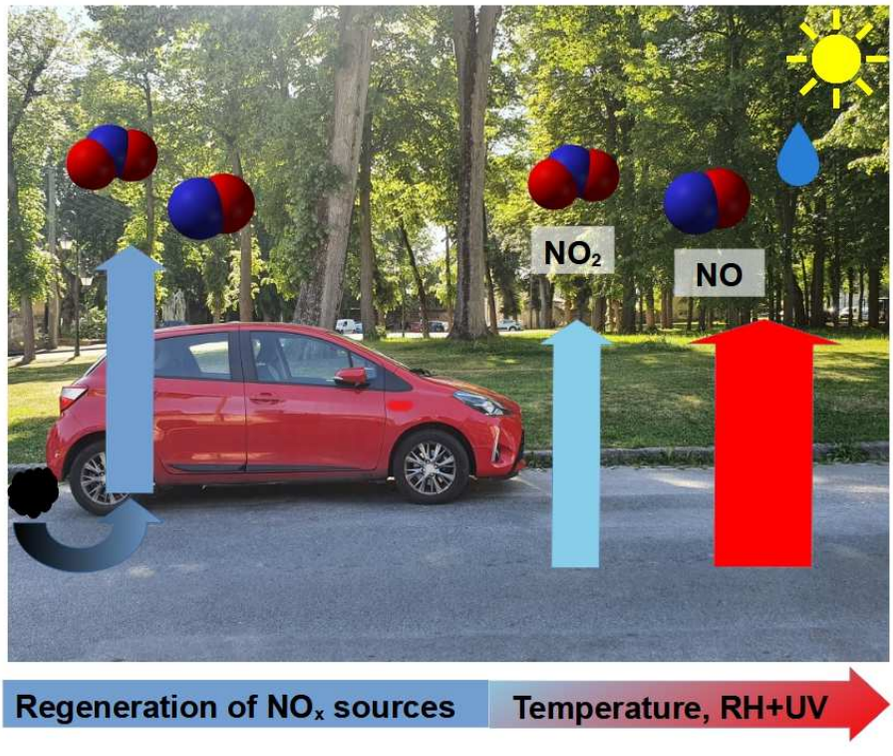

Abstract: Air pollution causes chronic illnesses, and an estimated 4.5 million deaths every year. 70% of mankind is expected to live in cities by 2050, making urban areas key for air quality and related health issues. These areas are largely covered with asphalt pavements. Pollutant emissions from asphalts are generally investigated at 120-160°C, temperatures that are reached during deposition of

asphalt mixtures, but data at in-use temperatures are lacking. In the present work, we characterize and quantify in the laboratory emissions of nitrogen oxides (NOx = NO+NO_2) by fresh and old asphalt mixtures under simulated atmospheric conditions. The impact of asphalt aging on NOx emissions is assessed, and the regeneration of NOx emissions by exposure of asphalt to the gas exhaust of a car is evidenced experimentally. With a numerical model of NOx emissions in Athens, Greece, we show that this previously unknown source accounts for up to 20% of NOx emission in specific locations. Asphalt-covered surfaces can therefore significantly contribute to NOx urban pollution, and need to be included to emission inventories, and taken into account by models for a better understanding and description of factors influencing urban air quality.

Keywords: Atmospheric Pollution; Urban Air Quality; NOx; Emissions; Asphalt Mixtures.

1. Introduction

The global death toll of air pollution is estimated at 8.8 million deaths per year, with an average life expectancy loss of 3 years [Lelieveld *et al.*, 2020]. Recent estimates suggest that outdoor air pollution accounts for 4.2-4.5 million deaths every year [Health Effects Institute, 2020]. Air pollution is exacerbated in cities, where pollution sources are numerous and located in a restrained area. Moreover, the urban proportion of global population is growing, from around 50% today to a projected 70% of mankind living in cities by 2050 [UN DESA, 2019]. Air quality and its impact on health are therefore major challenges of our time, and their importance can be expected to grow in a future challenged by climate change.

Air pollution can affect living beings and the environment in several ways. Greenhouse gases, such as carbon dioxide, increase Earth's surface temperature. Oxidants, such as ozone (O_3), and their precursors, nitrogen oxides (NOx) and Volatile Organic Compounds (VOCs), are irritant and toxic species, causing airway inflammation and increased respiratory symptoms in people suffering of asthma. NOx and O_3 are key species regulating atmospheric chemistry [Finlayson-Pitts and Pitts, 1993], [Atkinson, 2000], and dominant pollutants in cities [Sillman, 1999]. Their nighttime and daytime cycles are linked, and dictate pollution levels in urban areas. Models predicting the concentrations of these species are fundamental, but usually focus on traffic exhaust emissions (see, *e.g.*, [Fameli and Assimakopoulos, 2015]), the assumed major source of chemical and particulate pollutions in cities. However, models of urban atmospheric chemistry largely underestimate observed NOx concentrations, by 50% in most cases [Kim *et al.*, 2018], [Kuik *et al.*, 2018], [Oikonomakis *et al.*, 2018], [Ramacher *et al.*, 2021]. A major urban NOx source is therefore missing from inventories.

Paved surfaces represent more than 40% of urban areas [Akbari *et al.*, 2003]. The role of asphalt materials in the urban heat island (UHI) phenomenon, and as an impervious surface hindering rainfall infiltration, is well-established [Li *et al.*, 2019]. Several studies have investigated asphalt mixtures at deposition temperature (*i.e.*, T > 120-140°C), and the impact of aging caused by oxidation under extreme environmental conditions on the physical properties, chemical composition and chemical structure of asphalts [Lesueur, 2009], [Hofko *et al.*, 2018], [Villegas-Villegas *et al.*, 2018]. These studies stress the strong influence of UV radiation, humidity and temperature on asphalt aging [Villegas-Villegas *et al.*, 2018]. These factors likely also influence the chemistry occurring at the surface of asphalt pavement, and hence emissions of chemicals by asphalt binders are also expected to be sensitive to these parameters.

Emission of primary atmospheric pollutants by asphalt mixtures at deposition temperatures higher than 120-140°C is now reasonably well constrained, at least regarding Polycyclic Aromatic

Hydrocarbons (PAHs; see, *e.g.*, [Nilsson *et al.*, 2018], [Cavallari *et al.*, 2012a], [Cavallari *et al.*, 2012b], [Preiss *et al.*, 2006]) and VOCs (see [Espinoza *et al.*, 2020], [Gasthauer *et al.*, 2008], [Borinelli *et al.*, 2020]). However, the impact of asphalt surfaces on urban air quality at atmospheric relevant temperatures has been overlooked and is, at present, largely unknown. To our knowledge, only a single study focused on VOC emissions of fresh asphalt at relevant in-use temperatures [Khare *et al.*, 2020]. Asphalt emissions are shown to be a major source of VOCs [Khare *et al.*, 2020], which contribution to urban air quality needs to be precisely assessed as it may significantly contribute to the background levels of VOCs considered in models.

In light of these findings, the large surface provided by road-coating asphalts may also participate in urban NOx emissions. Indeed, nitrogen- and oxygen-bearing species are naturally present in bitumen [Lesueur, 2009], and in their emissions [WHO IARC, 2013]; diesel and gasoline vehicles' exhaust contain numerous NOx-bearing species [WHO IARC, 1989], that may remain on the surface of asphalt pavement and provide a prolific, extended and constantly renewed NOx source. NOx emissions by urban surfaces such as asphalt pavements could be the missing source needed by atmospheric models to adequately simulate field observations of urban environments.

In this paper, we set out to quantify experimentally, with an atmospheric simulation chamber, NOx emissions by real-world asphalt samples to complete inventories, and provide models of urban atmospheric chemistry with a new extended source. These data feed the respective numerical model experiments, to quantify the impact of NOx from paved road surfaces on the concentration levels at the city scale.

2. Materials and Methods

2.1. Origin and Characterization of the Samples

We investigate asphalt samples used for road pavement in Douai, a medium-size city located north of France in the area of Lille metropolis, a densely urbanized area of 7200 km^2 populated by 3.8 million inhabitants. The fresh asphalt mixture samples were obtained from an asphalt plant (STA7 to STA9; AC 10 mixture according to EN 13108-1, corresponding to a French BBSG 0/10 made with limestone aggregate and 35/50 penetration grade bitumen), or collected on-site during deposition in Douai in 2018 (STA3, STA4; BBTM 10A according to EN 13108-5 made with porphyre aggregate and 35/50 penetration grade bitumen). The fresh asphalt samples have therefore not experienced weathering before the experiments, but short-term aging (STA) as defined in [Lesueur, 2009]. The collected samples (STA3 and STA4) have been subsequently stored in the lab under clean conditions for two years before they were used in experiments. Emissions from these samples should therefore be compared with long time emissions from the samples used in [Khare *et al.*, 2020], that were used shortly after collection. Old asphalt samples (LTA5 to LTA8) were collected during road resurfacing works of a street in the city centre of Douai (rue de Bellain; 50.3689°N, 3.0823°E) in March 2021. The asphalt pavement layer was deposited in 1992, and has therefore been in service for almost 30 years under a slow traffic close to 5,000 vehicles per day, with 5% of heavy vehicles. Moreover, it has been weathered under real-life conditions (summer/winter temperature cycles, day/night light cycles, rainfall, gas exhaust of automotive vehicles, etc.), resulting in long-term aging (LTA) [Lesueur, 2009]. More details on the samples used are available in **Table S1** of Supplementary Information. These two types of "real-world" samples provide good representations of fresh and aged road pavement, and are therefore appropriate to evaluate asphalt emissions in urban areas based on experimental data obtained on real samples.

Before they can be used in the experiments, the STA samples are cut into rectangular cuboids. STA asphalt samples are not subjected to any further treatment prior to their use in the

atmospheric chamber. LTA asphalt samples are cut into rectangular fragments (roughly 20 cm x 8.5 cm) with a thickness of 1.3-1.7 cm suggesting that the emissions come from the oxidized asphalt layer composing the road surface. The LTA asphalt samples are flushed with dry air and gently washed with water to remove road dust before use in experiments.

2.2. Environmental Conditions Experienced by Road Asphalt Mixtures

Temperatures lower than 70°C are relevant for road surfacing during most of its lifetime under typical weather conditions experienced at mid-latitude and low-latitude regions, where asphalt surface temperatures can reach 60°C under sunlight during a hot day [Toraldo *et al.*, 2015], [Higashiyama *et al.*, 2016], [Solatifar *et al.*, 2018], [Parison *et al.*, 2020]. In the context of global warming associated to climate change, asphalt temperatures as high as 50-60°C cannot be considered exceptions anymore, and are common over summer. We have actually measured elevated asphalt temperatures at the surface of the parking lot facing our laboratory with an infrared thermometer. On typical summer days in Douai, north of France (50°22'17"N, 3°04'48"E), we recorded asphalt temperatures between 16.4°C and 52.2°C under the sun. During these measurements, air temperature ranged between 19.0°C and 32.8°C, relative humidity between 32% and 51%, and wind speed between 0 and 14.4 km h^{-1}, as measured by the weather station located on the roof of the building hosting our laboratory (data presented in **Table S3** of Supplementary Information).

2.3. Experimental Setup

Figure 1 shows a schematic representation of the experimental setup. A 20 L Teflon chamber sits in a Memmert UF110 chamber used to regulate the temperature of the sample. Zero air is supplied by a Claind AZ 2020 generator and split into two flows, regulated by Mass Flow Controllers (MFC; MKS Mass-Flo© controller, respectively 1000 and 2000 sccm, standard cubic centimeter per minute); the MFCs are controlled by a four-channel MKS type 247 readout unit. One part of the flow goes through a bubbler filled with ultrapure water (milli-Q, resistivity 18.2 MΩ cm), and is later mixed with the dry air flow to reach the degree of relative humidity (RH) desired that is continuously monitored with a Kimo KT 220 O RH probe. The total flow, sent in the chamber via a Teflon tube, is in the 2055-2320 sccm range. The Reynolds number of the flow in the chamber is Re ≈ 21826-24636, ensuring that the flow is turbulent, hence that the emissions of the asphalt mixtures are well mixed in the chamber, and that the air sample is not biased by a concentration gradient effect.

Two UVA lamps (Philips PL-L 18W/10/4P; 315-400 nm, with maximum emission at 352 nm) are placed on both sides of the Teflon chamber to simulate solar UV radiation. Measurements of the photolysis rate of NO_2 in the chamber lead to $J_{NO2} = 1.5\times10^{-3}$ s^{-1} (measured in separate experiments), a value at the lower regime of J_{NO2} measurements in the atmosphere of Earth under cloudy and clear sky conditions [Barnard *et al.*, 2004], [Bohn *et al.*, 2005], [Topaloglou *et al.*, 2005]. The ratio of the total flow to the volume of the chamber provides a residence time below 10 s in the chamber, making NO_2 photolysis by UV-lamps negligible. Emissions of the asphalt samples are collected with the air flow downstream of the chamber.

Nitrogen oxides (NO, NO_2, and NOx) are detected with a Teledyne T series NO-NO_2 analyzer T200UP (limit of detection = 50 ppt; intake flow rate = 1100 sccm). With this instrument, NO_2 is measured photolytically without interference with other nitrogen-bearing species of interest, such as nitrous acid (HONO) [Romanias *et al.*, 2020]. The calibration of the instrument was achieved in the frame of ACTRIS (Aerosol, Clouds and Trace gases Research InfraStructure) [Reimann *et al.*, 2018]. Note that alkenes may interfere with the measurement of NOx concentrations by chemiluminescence. Alkenes emitted by asphalt mixture samples in the chamber, are collected in a Carbotrap 202 tube, and subsequently analyzed offline with GC-MS/FID (Gas Chromatography - Mass Spectrometry / Flame Ionization Detector; 7890A GC system, Agilent Technologies). Under our

experimental conditions, alkenes concentration is always below 2 ppb, and is constant 1 hour after heating the sample or exposing it to UV-irradiation. Alkenes concentration below 2 ppb warrant that interference with NO measurements are below 1% of the signal [Alam *et al.*, 2020], and may be neglected. The GC-MS/FID results dealing with VOC emissions by asphalt mixes are beyond the scope of the current paper, and will be presented separately. In addition, ozone levels are measured with a Horiba APOA-370 instrument (limit of detection = 50 ppt; intake flow rate = 700 sccm).

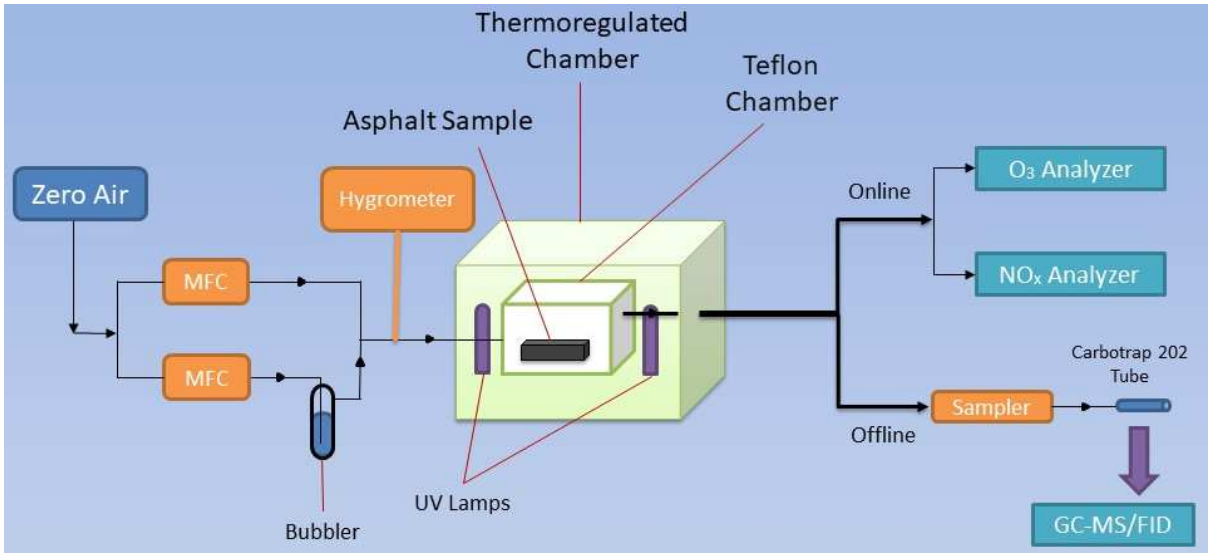

Figure 1: Schematic representation of the experimental setup. A dry zero air flow, and a humid air flow are regulated with mass flow controllers (MFC), mixed and flowed in the Teflon chamber sitting in a thermoregulated chamber. Two UVA lamps are located on each side of the Teflon chamber for UV- irradiations. The vector gas injected in the chamber carries the emissions of the asphalt sample out of the chamber, where it is analyzed online by the NOx analyzer, and an O_3 analyzer. A sampler is used for GC-MS analysis.

2.4. Determination of the Emission Factors (EF)

In the following, emissions are given as Emission Factors (EF). EF values (in µg m^{-2} h^{-1}) are obtained by converting the measured concentrations C (ppb, part per billion) of a species of molar mass M (g mol^{-1}), into mass emissions per area of asphalt and per time unit. EFs account for the Emitting Geometric Area ($S_{asphalt}$, in m^2) and temperature (T, in°C) of the sample, and the flow of the bath gas in the Teflon chamber, Q_e (in m^3 h^{-1}), as shown in Equation (1), commonly used in calculations of emissions from materials [Caron *et al.*, 2020].

$$EF = C \times 12.187 \times \left(\frac{M}{273.15+T}\right) \times \frac{Q_e}{S_{asphalt}} \quad (1)$$

The determination of an intensive parameter, such as EF, allows comparison of different experiments, of experiments with different samples, and of experiments conducted under different physical conditions. Such comparison would not be possible with raw concentrations; hence, in the following we discuss EFs values calculated with (1).

2.5. Setting up the Numerical Model Simulations

The numerical atmospheric model system selected for this study is schematically represented on **Figure 2**. The core of the system is the chemistry transport model EPISODE-CityChem [Karl *et al.*, 2019]. The model is carefully selected to accurately represent the atmospheric pollution conditions on road and over the adjacent urban areas, which is the main focus of this study.

Specifically, the model is fed with hourly road network emissions in a linear format, applies a Gaussian dispersion scheme in the street canyons, and an extra photochemical scheme over the greater area of road surfaces, gridded in 100m-by-100m cells. These two schemes are superimposed to the Eulerian treatment of atmospheric processes in the whole 3D urban domain, with a horizontal spatial resolution of 1 km and a 24-layered atmosphere up to 3.7 km.

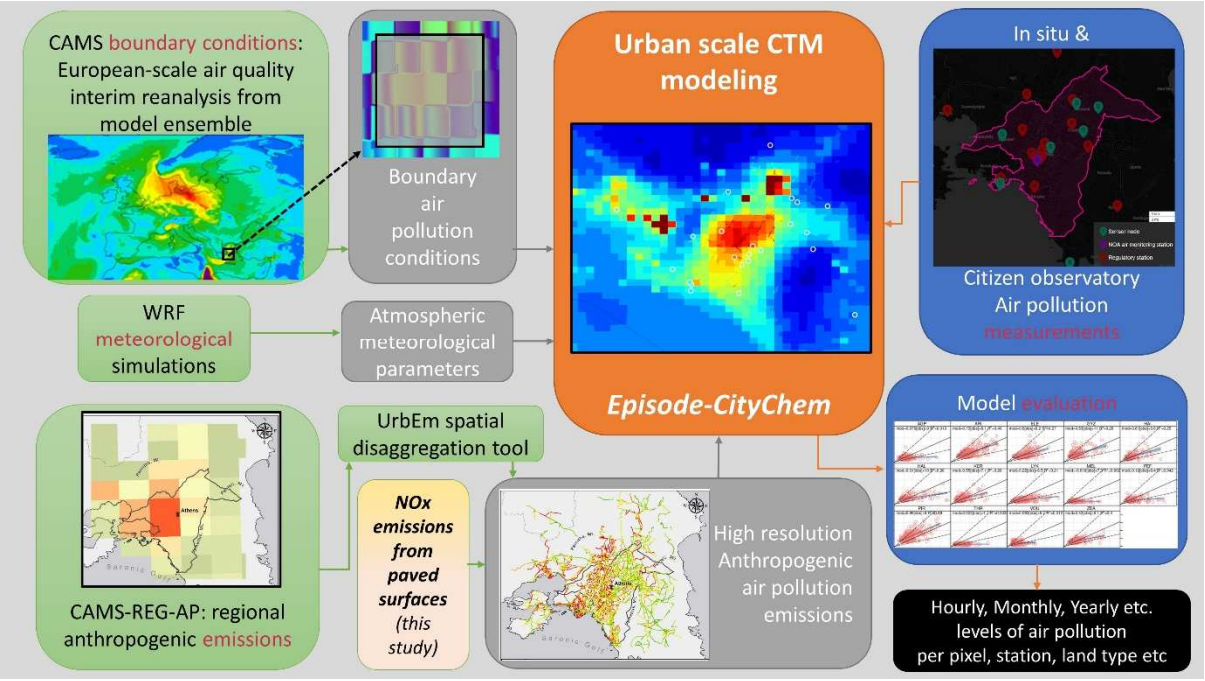

Figure 2: The atmospheric numerical model system used in this study. More information on the model configuration and setup can be found in Supplementary Information.

Although the samples used in experiments originate from the city of Douai, France, the numerical model of NOx emissions by asphalt pavements is applied to Athens, Greece, as pilot city. There are several reasons for this choice:

- The age of the old LTA asphalt samples collected in Douai match that of the network of the city of Athens city center. Even if local materials and aging conditions are known to be somewhat different, we hypothesize that emissions of LTA samples are also representative of old asphalt mixtures in Greece;
- Both temperature and light irradiation conditions applied in the chamber experiments are relevant for Athens;
- In a context of growing urbanization, and degradation of urban air quality, assessing the impact of asphalt pavements on urban pollution seems more relevant if studied in a large urban area, such as Athens;
- Athens has a dense road network, allowing us to better evaluate the impact of asphalt pavements on urban air quality;
- Athens has detailed and reliable pollution monitoring data, with high spatial and time resolution, easily accessible to the scientific community (*e.g.*, Copernicus Atmosphere Monitoring Service, CAMS), which is not the case for the city of Douai;
- The model setup and performance have already been described and tested in Athens [Ramacher *et al.*, 2021].

The studied period (September 2019) has been carefully selected to represent the environmental conditions described in **section 2.2**, prior to the COVID-19 lockdown period.

Anthropogenic emissions are originally provided by CAMS, and then improved over the domain of interest with the spatial disaggregation approach and tool documented in [Ramacher *et al.*, 2021]. Conventional road emissions correspond to gases and particles from the vehicle exhausts, provided as hourly mass emission rates by each road link of the city. For the current study, asphalt NO and NO_2 emissions are added, using the daily emission profile per surface unit provided by the atmospheric chamber experiments, and multiplied with the surface of each road link, as derived by the relevant data of the Open Street Map (OSM) database. **Figure 3** shows the mapping of mean monthly NO_2 emissions from asphalt, compared to the quantities emitted from vehicle exhausts. The base-case model simulation is based on conventional emissions, while the impact of asphalt is assessed through NO_2 concentration differences from a scenario with input from both sources. As evidenced by a comparative overview of the linear emissions by cars and asphalt, the mass emitted by vehicle exhausts in the inner city center is about two orders of magnitude higher than that emitted by paved surfaces. For the suburban road network, this difference is reduced to differences by a factor of 2 or less, both due to less traffic and larger road surfaces.

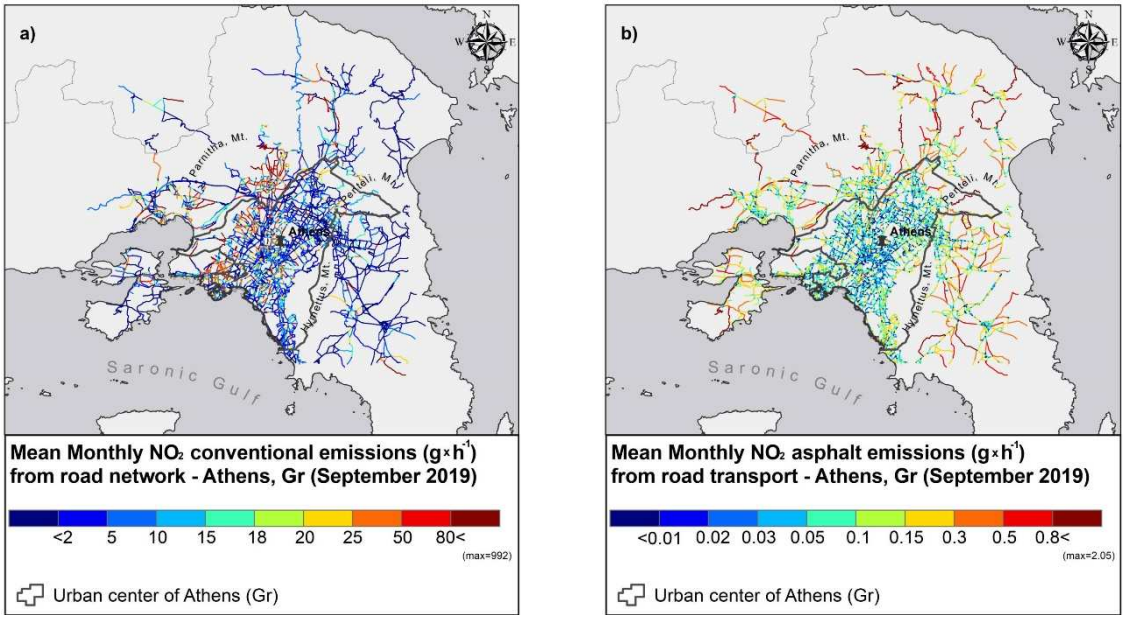

Figure 3: Mean monthly (September 2019) anthropogenic NO_2 emission fields (g h^{-1}) from a) vehicle exhausts and b) road asphalt, of the Athens basin (Greece).

3. Results and Discussion

Nitrogen oxides (NO, NO_2, and NOx = NO+NO_2) emissions of STA and LTA asphalt mixture samples are measured between 23°C and 60°C, under different conditions of relative humidity (RH), in the dark and under UV light. **Sections 3.1 to 3.6** present the experimental results from the atmospheric chamber experiments to unravel the impact of atmospheric conditions on NOx emissions by asphalt pavements. **Sections 3.7** deals with the implementation of experimental results in the city-scale model, to elucidate their implications for urban air quality.

3.1. Experimental Data

An example of the NO, NO_2 and NOx EFs calculated with (1) from data of a typical experiment are presented on **Figure 4**; NO, NO_2 and NOx concentrations recorded during the experiment are shown on **Figure S1**. In this experiment at RH = 57%, the LTA8 asphalt mixture

sample is exposed to temperatures of 35°C and 50°C successively, in the dark, and under UV-irradiation at 50°C. At each temperature increase of the thermoregulated chamber, 30 to 60 minutes are necessary for the sample to reach thermal equilibrium, as controlled with measurements of the sample's surface temperature with an infrared thermometer. **Figure 4** shows the challenges related to the measurement of NOx EFs by asphalt samples. Emissions vary with temperature, light irradiation, and purging time. Therefore, it is necessary to describe the emission kinetics of the samples at each temperature and condition.

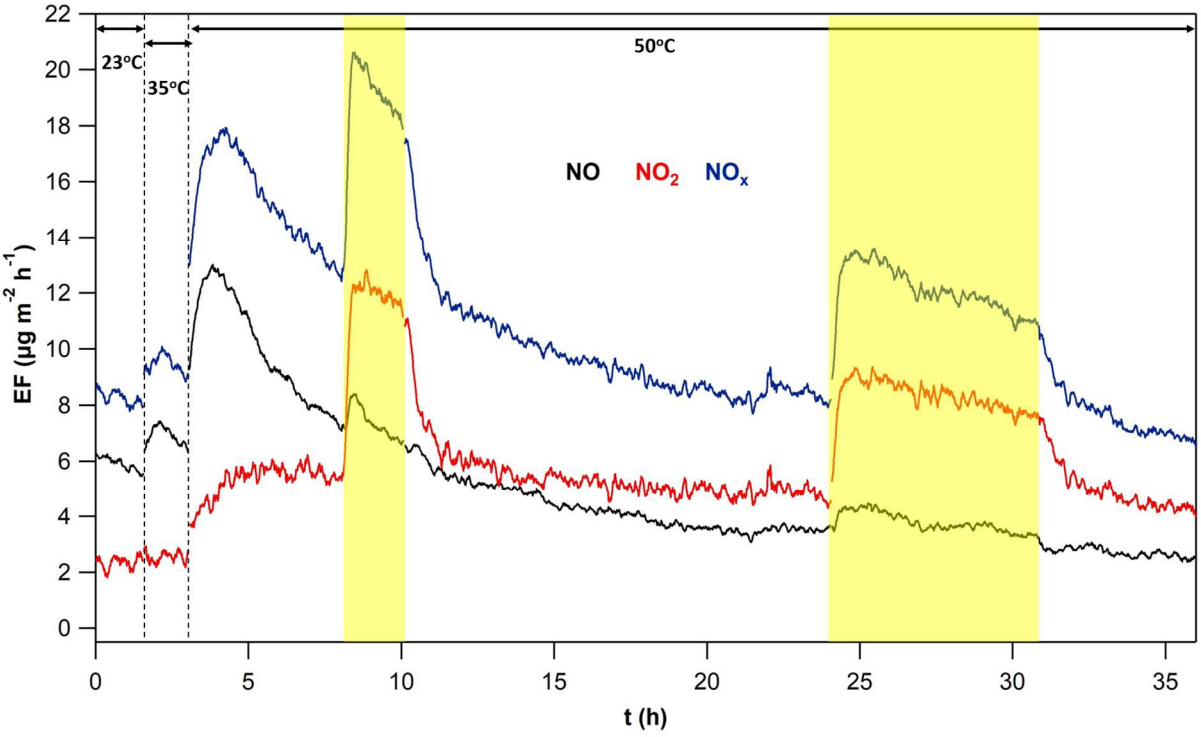

Figure 4: NO (black), NO_2 (red), and total NOx (blue) EFs (in µg m^{-2} h^{-1}) emitted by the LTA8 asphalt sample at RH = 57%, as a function of time. Yellow-shaded areas indicate UV-irradiation (J_{NO2} = 1.5 × 10^{-3} s^{-1}); the experiment takes place in the dark otherwise.

3.2. Emission Kinetics

In this section we discuss NO and NO_2 emission kinetics of old (LTA, **section 3.2.1**) and then fresh (STA, **section 3.2.2**) asphalt mixtures. At the end of **section 3.2** we briefly discuss the differences noted between old and fresh samples.

3.2.1. Emission Kinetics from LTA Asphalt Mixtures

NO Emission Kinetics

T = 23°C: NO emissions are stable during the first 40 hours under humid zero air (only the last 1.5 h are shown on **Figure 4**). For experiments collecting emissions for longer than 100 hours, they can be lower by a factor of up to two.

T = 35°C: As shown on **Figure 4**, EF_{NO} seems to peak after annealing to 35°C, and then to decrease. Although we have been able to measure maximum (peak) and minimum (steady-state) values of EF_{NO} at 35°C in the dark, we focused on more relevant values, such as T = 50°C presented below.

T = 50 °C: **Figure 5** shows EF_{NO} in the dark as a function of time t = 0 is chosen as 60 minutes after the thermoregulated chamber is set to 50°C. This conservative value is long enough to make sure that the samples have absorbed and homogeneously distributed the thermal energy provided, and reached 50°C, as discussed earlier. When the temperature of the chamber increases, EF_{NO} peaks 1-2 hours after the asphalt temperature is stable. Experimental EF_{NO} values are fitted with bi-exponential functions according to Equation (2); the result is shown on **Figure 5**. The match of the fits with the experimental data remains in very good agreement even after experimental steps with different parameters take place (missing points on **Figure 5** that correspond to UV-irradiation of the sample, see also **Figure 4**). This gives confidence in the extrapolation of the kinetics based on the fits.

$$EF_{NO}(t) = EF_{NO}(40h) + A_1 exp^{-k_1 t} + A_2 exp^{-k_2 t} \quad (2)$$

k_1 = 0.045 h^{-1}, k_2 = 0.31 h^{-1}, and EF_{NO}(40h) = 1.40±0.30 µg m^{-2} h^{-1} are deduced from the fits. EF_{NO}(40h) corresponds to a steady-state value after 40 hours of collection of the emissions. The uncertainty on EF_{NO}(t) includes the precision of the signal and the dispersion of the values of EF for different samples tested (discussed also in **section 3.3**). However, it should be noted that over longer timescales (100 h) of collection of NOx emissions under zero air, we observe a reduction of the steady-state value to EF_{NO}(100h) = 0.80±0.25 µg m^{-2} h^{-1}. Given the experimental uncertainties, it is close to EF_{NO}(40h). Furthermore, we find A_1/A_2 = 1.7±0.4; this ratio is constant, as confirmed with different samples examined. Knowing that EF_{NO}(40h) + A_1 + A_2 = EF_{NO}(peak), one may determine the full kinetics, *i.e.*, EF_{NO}(t), from the measurement of only EF_{NO}(peak).

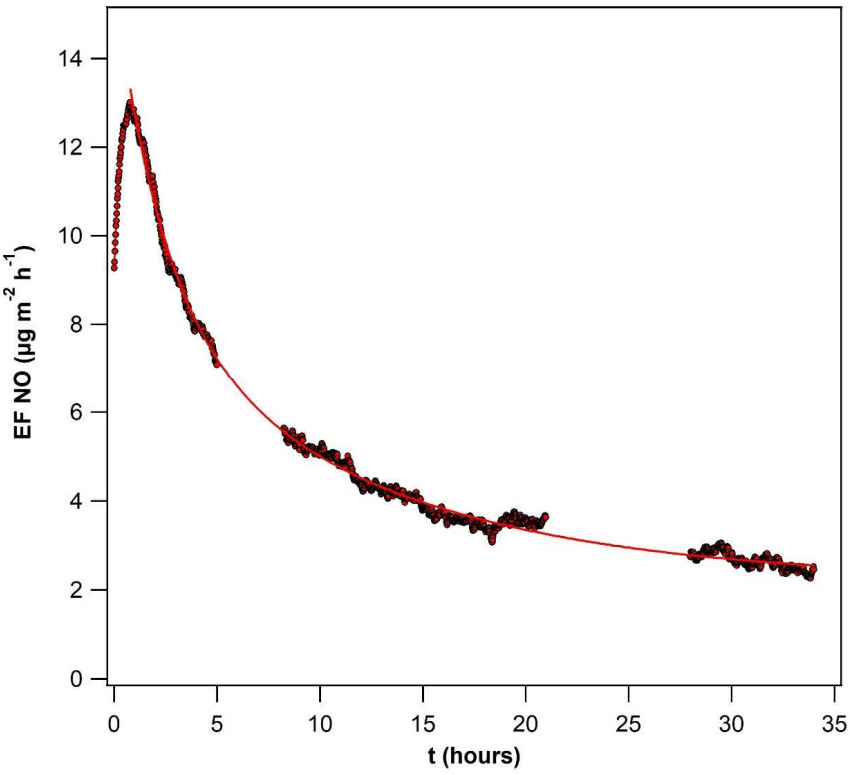

Figure 5: Experimental EF_{NO} of the LTA8 sample heated to 50°C for the first time, at RH = 57% and in the dark, as a function of the time spent by the sample at 50°C (black points). The red line shows the fit of the experimental data with a bi-exponential function. Datapoints corresponding to different experimental conditions (UV irradiation) have been omitted.

We now turn to the discussion of these experimental observations. The fast and large initial increase of EF_{NO} after each temperature increase suggests the presence of a thermally-induced source of NO at the surface of LTA asphalt. The global emission of NO decreases and eventually reaches a steady-state. EF_{NO} does not go zero though, but is sustained over at least 34 hours (see **Figure 5**). Hence, the source of NO is not depleted over timescales longer than 24 hours. We have not monitored the full kinetics of emissions under UV-irradiation from the beginning, but always after a temperature change, so direct comparison with a temperature increase is difficult. UV-irradiation seems to produce a more modest change of EF_{NO} than a temperature increase, and the concomitant increase of EF_{NO2} is stronger than during a temperature increase (see **Figure 4**). The slight variation of EF_{NO} under UV radiation can be linked to heterogeneous or gas-phase photochemistry of NO_2 in the chamber.

In the dark, after the peak of EF_{NO} is reached, the decrease phase is composed of two exponential functions (**Figure 5**), with characteristic times of 3.2 h and 22.2 h. It points to NO emissions being caused by a "fast" channel, with a characteristic time of ≈ 3.2 h, and a "slow" channel, with a characteristic time of ≈ 22.2 h. These two channels may be linked to two types of NO sources being present at the surface of asphalt, or to two types of processes, emitting NO according to two different kinetics upon increase of the temperature.

NO_2 Emission Kinetics

T = 23°C and 35 °C: NO_2 emissions are stable within the first 40 hours. For experiments longer than 100 hours under humid zero air, they can be lower by a factor of up to two.

T = 50°C: In the dark, EF_{NO2} remains almost constant within the first 40 hours of the experiments. Under a flow of clean humid air for more than 100 hours, we note that EF_{NO2} can decrease by a factor of two. Under UV-irradiation at 50°C, **Figure 4** shows that EF_{NO2} increases sharply when the UV lamps are switched on, before it decreases slowly with time. Fits of the experimental data show that EF_{NO2} decays exponentially, following Equation (3).

$$EF_{NO2}(t) = EF_{NO2}(peak) \times e^{-k_3 t} \quad (3)$$

For LTA samples at 50°C, we find $k_3 = 0.02\ h^{-1}$. This is equivalent to a characteristic decay time of NO_2 emissions of 50 hours, meaning that EF_{NO2} can be considered constant over a day under UV-irradiation at a fixed temperature.

3.2.2. Emission Kinetics from STA Asphalt Mixtures

Regarding STA samples, observed EF_{NO} and EF_{NO2} are almost always constant in the dark at each temperature step investigated. In few instances, a peak followed by a slow decrease is observed for one out of the three samples studied; however, the difference between peak and plateau is not significant due to the relatively low level of EFs. Hence, NO and NO_2 emissions by STA asphalt in the dark may be regarded as constant at any fixed temperature, suggesting that the emissions of STA samples reach a steady-state directly, without a transition regime. This is in contrast with the behavior of LTA asphalt described in the previous section. An example of such a behavior is shown on **Figure S2** in Supplementary Information.

The first irradiation of an STA sample with UV photons leads to a peak of EF_{NO} and EF_{NO2}, followed by a decrease. Fits of the experimental data at 50°C show that EF_{NO} and EF_{NO2} decay exponentially under UV-irradiation, following Equation (3). After 5h of UV-irradiation, EF_{NO} and EF_{NO2} reach a plateau. However, for experiments longer than 24 hours, plateau values can be lower by a

factor of up to two. The fits of the experimental data with (3) give k_3 for each experiment. k_3 seems to depend on the sample considered; for STA3&4 samples, k_3 = 0.65 h^{-1}, and for STA7&8, k_3 = 1.11 h^{-1}. These values are much higher than for LTA (0.02 h^{-1}), indicating a much slower kinetics for NO_2 emissions of LTA asphalt under UV-irradiation with respect to STA asphalt. The higher intensity of the emission peak caused by UV-irradiation of LTA asphalt with respect to STA asphalt indicates a significantly larger source of NO_2 in LTA, and that this source is photo-decomposed to release NO_2 in the gas phase.

Another important finding is that only the first UV-irradiation produces a peak followed by an exponential decay, regardless of the temperature; it has been observed at 35°C and at 50°C, in experiments on two different samples at 50°C. The next UV-irradiations of the samples do not produce any peak of EFs, but lead to plateaus at 50°C and at 60°C. It suggests that the first UV-irradiation could modify and passivate the surface of asphalt against UV-irradiation before the surface is regenerated. The species on the regenerated surface are then sensitive to UV-irradiation again.

To summarize, comparison of EFs from different samples, different experiments, and even at different experimental steps of an experiment, requires the clear definition of EF values. For species reaching a plateau without peaking, only the steady-state value is accessible, and represents a minimum of EF; no maximum EF may be determined. Steady-state EF is calculated by averaging the signal over 1 hour at plateau. Maximum EF is calculated by averaging the signal over 1 hour centered on the emission peak. This is how we calculate the EF values presented in the following of the paper.

3.3. Variability of NOx Emissions between Samples

Emissions of STA and LTA asphalt mixture samples are measured at 23°C, 35°C, 50°C and 60°C. **Figure 6** shows the values of EF_{NO} and EF_{NO2} as a function of sample temperature, at RH = 57% and under dark conditions, for several STA (i) and LTA (ii) asphalt mixture samples. Error bars represent the standard deviation of the signal over the 1-hour average. For the temperature of 23°C and 35°C the EF_{NO} and EF_{NO2} corresponds to steady-state values, while for the temperature of 50°C and 60°C EF_{NO} represent max values and EF_{NO2} steady-state values.

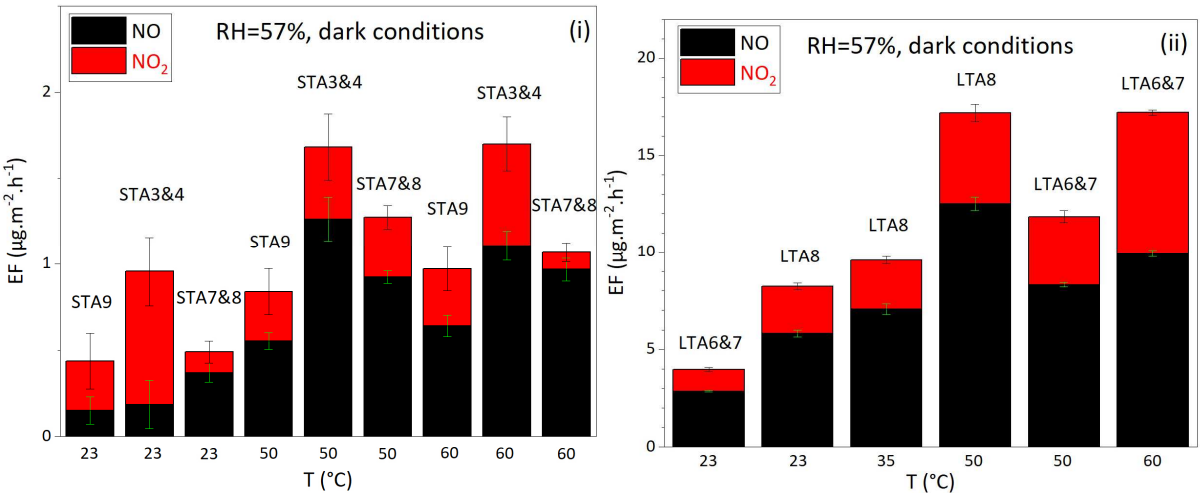

Figure 6: NO (black) and NO_2 (red) Emission Factors (EF) of (i) STA and (ii) LTA asphalt samples as a function of temperature, at RH = 57% and under dark conditions. Error bars arise from the dispersion of the experimental concentration. Note that the amplitude of the Y-scale differs by a factor of roughly 9 between the two figures.

Figure 6 presents EF values of different samples at various temperatures to highlight the spread of the individual values. Different samples do not necessarily exhibit the same emission pattern; **Figure 6(i)** shows that STA samples have total EFs in the 0.4-1 μg m^{-2} h^{-1} range at 23°C, but emissions are mostly composed of NO_2 for STA9 and STA3&4, while dominated by NO for STA7&8. Moreover, we note that STA7&8 emit a large majority of NO at all temperatures, whereas other samples release a larger proportion of NO_2. Overall, we observe an increase by a factor of two of the total emissions of STA samples with temperature, from 0.4-1 μg m^{-2} h^{-1} at 23°C, to 1-1.7 μg m^{-2} h^{-1} at 50°C and 60°C. Regarding LTA samples, EF values displayed on **Figure 6(ii)** are also spread at any given temperature due to the heterogeneity of the samples. Total NOx EFs increase markedly with temperature for LTA samples, from 4-8.2 μg m^{-2} h^{-1} at 23°C, to 17.2 μg m^{-2} h^{-1} at 60°C.

*Table 1: Average steady-state values (peak values are given in brackets) of EF_{NO} and EF_{NO2} for STA and LTA asphalt samples at different temperatures, RH = 57%, and under dark conditions. * indicates values determined with Equation (2). - indicates that there is no value to display. Quoted errors are the Standard Deviation of the average of the measurements, including those presented in Figure 4; they do not include the experimental error for individual measurements shown on Figure 4. Values for which no error is given are single experimental measurements, hence Standard Deviation is zero; nevertheless, considering the range of errors at other temperatures, a similar uncertainty can be anticipated.*

T (°C) **RH = 57%, dark**	EF_{NO} STA (μg m^{-2} h^{-1})	EF_{NO2} STA (μg m^{-2} h^{-1})	EF_{NO} LTA (μg m^{-2} h^{-1})	EF_{NO2} LTA (μg m^{-2} h^{-1})
23	- 0.24±0.12	- 0.39±0.34	- 4.33±2.09	- 1.77±0.91
35	- 0.34	- < 0.04	(7.05) 1.34	- 2.53
50	- 0.91±0.36	- 0.35±0.07	(10.41±2.46) 1.40±0.30*	- 4.11±0.82
60	- 0.91±0.24	- 0.34±0.25	(9.94) -	- 7.28

Comparison of average NO and NO_2 EFs of STA samples with those of LTA samples in **Table 1** shows that at any given temperature, LTA samples emit much larger quantities of NO and NO_2 than STA samples. At 23°C, total steady-state EF_{NOx} of LTA is 9.7 times larger than that of STA; at 35°C, 11.4 times; at 50°C, 4.4 times; and at 60°C, 6.9 times larger (taking the same value as at 50°C for the steady-state EF_{NO}). The larger NOx emissions of LTA with respect to STA is a first element pointing to the chemical aging of asphalt surfaces induced by exposition to traffic emissions and weathering, that could modify the chemical composition of asphalt and replenish the surface NOx reservoir. Other potential sources are discussed in more length in **section 3.5**. Even if the composition of both materials differed significantly (nature / gradation of aggregate, binder origin / content and overall porosity), the differences in EF are very pronounced, and suggest that long-term exposure to traffic and atmospheric weathering are responsible for most of the differences, as will be further detailed in **section 3.5**.

3.4. Influence of UV-Irradiation on NOx Emissions under Dry and Humid Conditions

A series of experiments are conducted under different conditions of relative humidity (RH = 0.1% or 57%), in the dark and under UV-irradiation, to determine the influence of gas-phase water and UV photons on NO_x emissions by STA and LTA samples. We irradiate the samples with two UV lamps (J_{NO2} = 1.5 × 10^{-3} s^{-1}) while the temperature inside the thermoregulated chamber is kept constant at 50°C. Indeed, the UV lamps used in our study, have low emission efficiency in the infrared region, and thus switching on or off the UV lamps does not cause any measurable temperature variation at 50°C, as confirmed by measurements of the asphalt samples' temperature with an infrared thermometer.

3.4.1. Under Dry Conditions (RH = 0.1%)

Figure 7 compares EF_{NO} and EF_{NO2} of STA6 (i) and LTA5 (ii) asphalt mixtures under dry conditions (RH = 0.1%), in the dark and under UV-irradiation at T = 50°C. For both types of sample, EF_{NO} remains stable (within error) after the sample is illuminated, whereas EF_{NO2} increases markedly. In the dark, LTA asphalt emits roughly 20 times more total NO_x than STA asphalt. Under UV-irradiation, total NOx emissions of LTA are approximately 8 times higher than those of STA, confirming than LTA asphalt is a more abundant NOx source than STA asphalt.

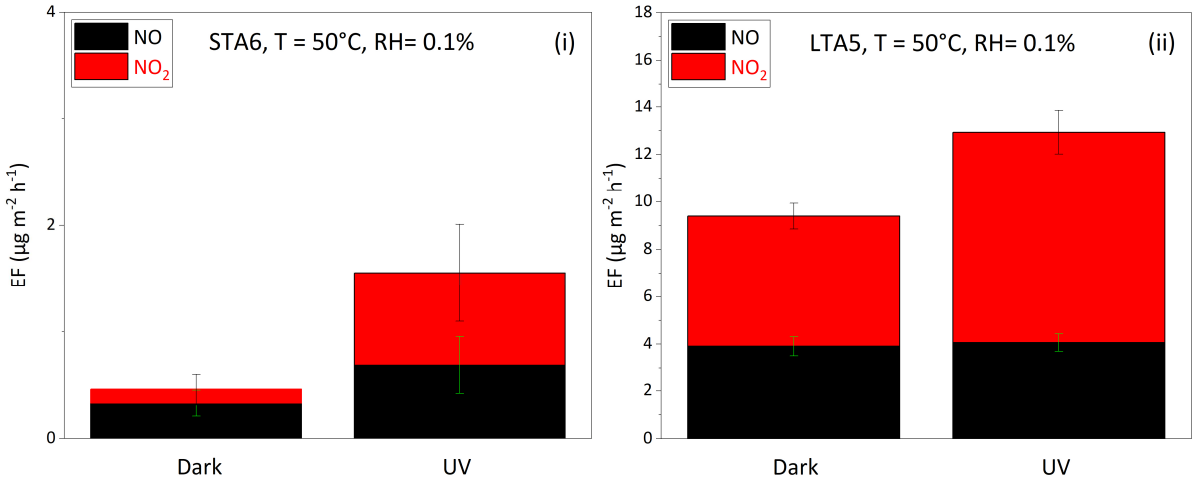

Figure 7: Effect of UV-irradiation on EF_{NO} (black) and EF_{NO2} (red) for STA (i) and LTA (ii) asphalts at 50°C under dry conditions (RH = 0.1%). Experiments are performed in the dark, and under UV-irradiation ($J_{NO2} = 1.5\times10^{-3}$ s^{-1}).

3.4.2. Under Humid Conditions (RH = 57%)

Figure 8 compares EF_{NO} and EF_{NO2} of STA (i) and LTA (ii) asphalts under humid conditions (RH = 57%), in the dark and under UV-irradiation at T = 50°C. For both STA and LTA, EF_{NO} remains stable within uncertainty when the sample is illuminated, whereas EF_{NO2} increases, as was observed under dry conditions with different samples. In the dark, LTA asphalt emits around 12 times more total NOx than STA asphalt. Under UV-irradiation, total NOx emissions of LTA are approximately 8 times higher than those of STA. This value is similar to that determined in dry conditions, but a direct comparison with these experiments is complex, because different samples are used. However, it confirms that under relevant environmental conditions, LTA asphalt is, by far, a larger NOx source than STA asphalt.

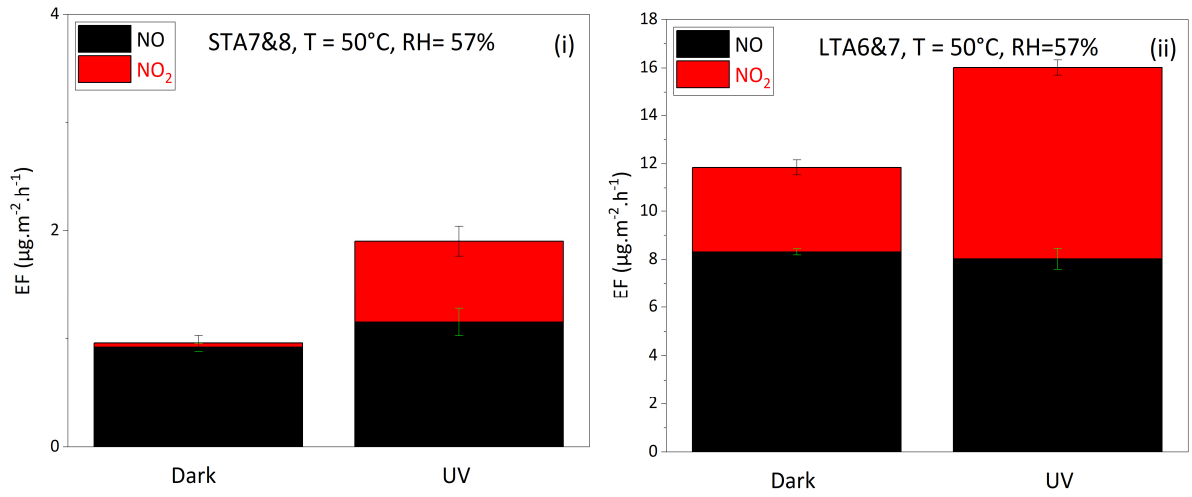

Figure 8: Effect of UV-irradiation on EF_{NO} (black) and EF_{NO2} (red) for STA (i) and LTA (ii) asphalts at 50°C under humid conditions (RH = 57%). Experiments are performed in the dark, and under UV-irradiation ($J_{NO2} = 1.5\times10^{-3}$ s^{-1}).

The data presented on **Figures 7** and **8** show that irradiation of STA and LTA asphalt samples with UV light increases NOx emissions at T = 50°C, both in dry and humid (RH = 57%) conditions. NO_2 especially is impacted by this process, whereas NO emissions are globally not sensitive to the presence of UV light.

*Table 2: Average steady-state values (peak values are given in brackets) of EF_{NO} and EF_{NO2} for STA and LTA asphalt samples at different temperatures, RH = 57% and under UV-irradiation. * indicates the values of EF(40h) determined from exponential fits of the data. - indicates that there is no value to display. Quoted errors are the Standard Deviation of the average of the measurements; they do not include the experimental error for individual measurements, shown on **Figures 5** and **6**. Values for which no error is given are single experimental measurements, hence Standard Deviation is zero; nevertheless, considering the range of errors at other temperatures, a similar uncertainty can be anticipated. ** indicates a value measured at 60°C, following a first annealing to 50°C; this value would certainly be higher if the first annealing was made to 60°C.*

T (°C) **RH = 57%, UV**	EF_{NO} STA (µg m^{-2} h^{-1})	EF_{NO2} STA (µg m^{-2} h^{-1})	EF_{NO} LTA (µg m^{-2} h^{-1})	EF_{NO2} LTA (µg m^{-2} h^{-1})
35	(2.30) 1.06*	(1.36) 0.45*	- 2.25	- 3.48
50	(1.26±0.16) 0.67±0.15*	(1.17±0.60) 0.59±0.30*	(10.41±2.46) 1.40±0.30*	(10.06±2.93) 4.52*
60	- 0.74±0.16	- 0.59±0.32	(6.21)** -	- 9.94

Table 2 presents averages of peak and steady-state EF_{NO} and EF_{NO2} values for STA and LTA asphalt under UV-irradiation at RH = 57%, at temperatures of 35°C, 50°C, and 60°C. It includes the values presented in **Figures 7** and **8**, additional experimental values, and values extracted from fits of the experimental data. We have controlled that at all temperatures investigated, the temperature of the samples remains constant under UV-irradiation. **Table 2** shows that under UV-irradiation, steady-state EF_{NO} and EF_{NO2} of STA asphalt remain almost constant with respect to temperature. Maximum emissions seem to decrease between 35°C and 50°C, but may actually remain constant if the standard deviation of the values could be included at 35°C. Regarding LTA asphalt, steady-state emissions increase with temperature; we note that they are extracted from single experimental measurements, hence no standard deviation can be calculated. Using a Standard Deviation of 20%,

typical of EF values in the dark at 50°C, suggests that steady-state EF_{NO} and EF_{NO2} of LTA under UV-irradiation increase between 35°C and 50°C, whereas they are stable between 50°C and 60°C.

3.4.3. Comparison of EFs in the dark and under UV-irradiation

Tables 1 and **2** allow comparison of NO and NO_2 emissions of STA and LTA asphalt at RH = 57%, and at temperatures between 23°C and 60°C, in the dark and under UV-irradiation. Comparison based on these tables is more general than the discussion of **Figures 7** and **8**, which relates on the evolution of specific STA and LTA samples subjected to UV-irradiation. Overall, EF_{NO} and EF_{NO2} are higher under UV-irradiation than in the dark for LTA asphalt. UV-irradiation does not seem to have a measurable impact on STA asphalt emissions. EF_{NO} and EF_{NO2} of STA are lower than LTA's, and are steady in the dark.

Interestingly, EF_{NO} and EF_{NO2} of STA asphalt exhibit, within error, similar values at the different temperatures investigated, both in the dark and under UV-irradiation. It suggests that, in the case of STA samples, which have not experienced traffic and weathering, there is no thermally-induced NOx source. Therefore, aging seems to play a key role on NOx emissions by asphalt surfaces.

Regarding LTA asphalt, steady-state values of EF_{NO2} is higher under UV light than in the dark. EF_{NO} however, has similar values in the dark and under UV-irradiation. It confirms that NO emissions are constant, and that the increase in NOx emissions caused by UV-irradiation are caused by an increase of NO_2 emissions. We note that EF_{NO} of LTA asphalt at 60°C is higher in the dark than under UV-irradiation. We suspect that the latter is underestimated, because the experiment at 60°C under UV-irradiation followed a first annealing to 50°C; NOx sources must have been depleted by the first annealing, leading to a value at 60°C lower than expected.

3.5. Regeneration of NO and NO_2 Emissions

We have established that LTA asphalt emits NOx years after its deposition; it actually produces stronger NOx emissions than STA asphalt. Hence, there must be one or several processes forming, or regenerating, the precursors of the NOx species emitted by asphalt. In this section, we set out to evidence regeneration of NOx emissions of LTA asphalt samples LTA6&7 by comparing NO and NO_2 EFs at 23°C in the dark (**Figure 9(i)**), at 50°C in the dark (**Figure 9(ii)**), and at 50°C under UV light (**Figure 9(iii)**). In a series of experiments, LTA6&7 samples are subjected to cycles at 23°C, 50°C in the dark and 50°C under UV light. Between the experiments, they are placed under conditions favoring or hindering the regeneration of their NOx sources, as described below.

(A) refers to the first experiment conducted on LTA6&7 samples, 2 months after they were collected. The total NOx Emission Factor, $EF_{NO}+EF_{NO2}$, obtained during this first experiment serves as reference (100%); it takes the following values: 3.97 µg m^{-2} h^{-1} at 23°C, 11.85 µg m^{-2} h^{-1} at 50°C in the dark, and 15.67 µg m^{-2} h^{-1} at 50°C under UV-irradiation. Experiment (B) is performed after the samples were left for 30 days in the lab's fume hood, wrapped in Teflon and in tin foil to prevent interaction with NOx sources of the outside environment. Experiment (C) is conducted after the samples were left for 4 days outdoors, under a cloudy weather (direct sunlight exposition was limited) at an ambient temperature of 16-28°C; the samples received a modest amount of sunlight during this period, and were located away from road traffic. Experiment (D) follows exposure of the samples to the exhaust of a diesel car for 45 minutes.

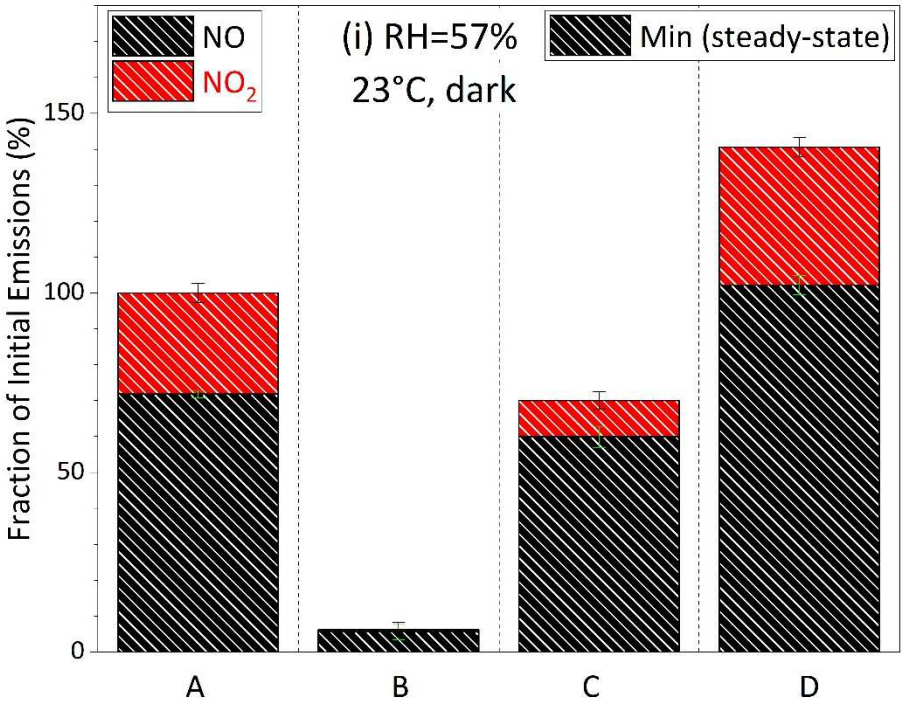
NO
NO2
(i) RH=57%
23°C, dark
Min (steady-state)
Fraction of Initial Emissions (%)
150
100
50
0
A
B
C
D

584

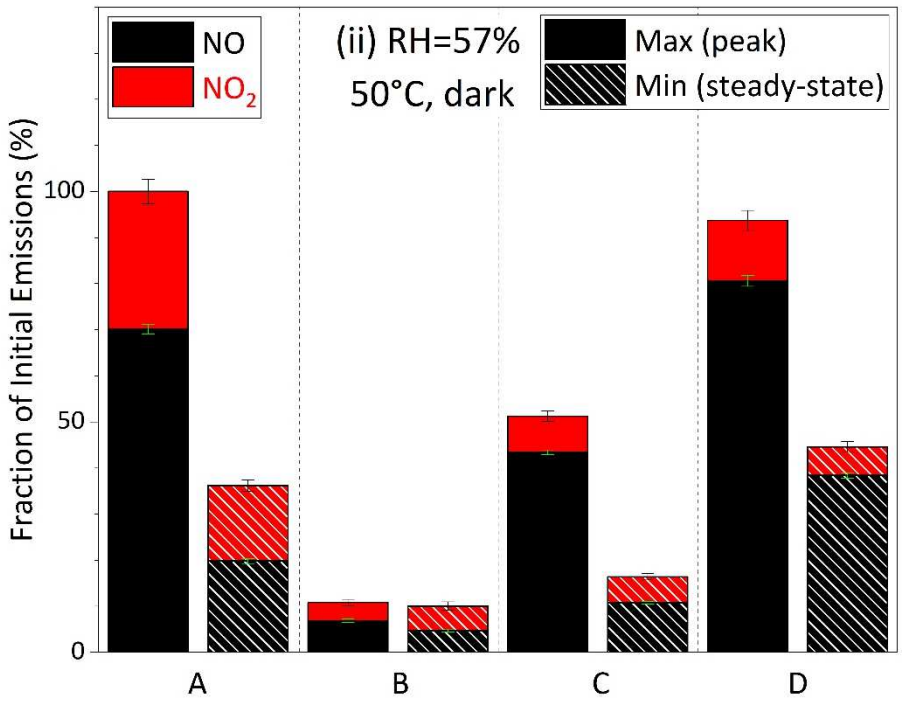
NO
NO2
(ii) RH=57%
50°C, dark
Max (peak)
Min (steady-state)
Fraction of Initial Emissions (%)
100
50
0
A
B
C
D

585

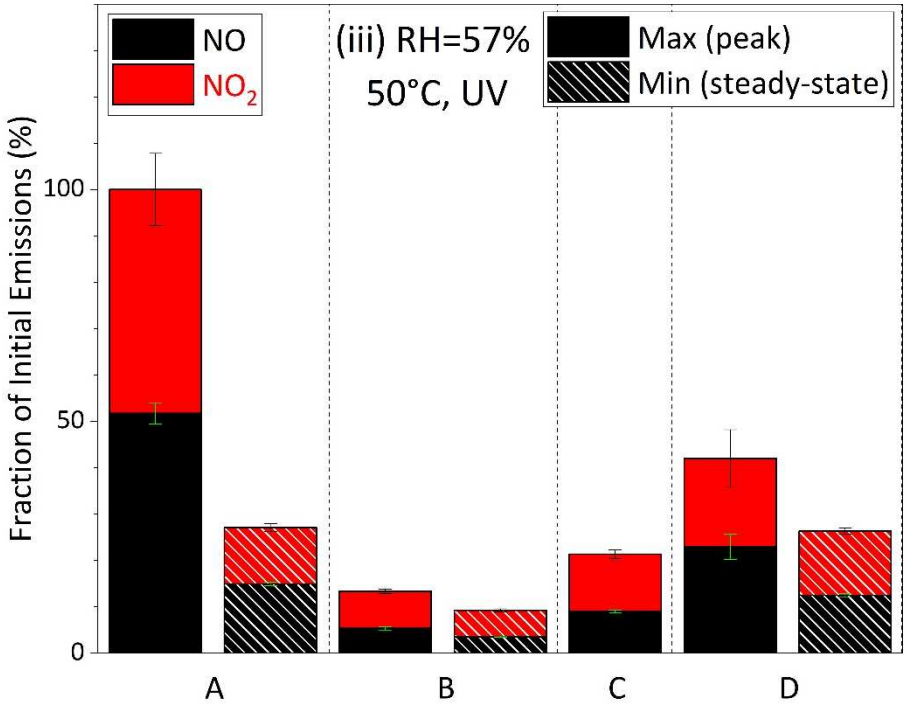

Figure 9: Peak and steady-state EF_{NO} (black) and EF_{NO2} (red) measured at 23°C (i), 50°C in the dark (ii) and 50°C under UV (iii) in a series of experiments on LTA6&7 samples. (A) First experiment with LTA6&7 samples; (B) After the samples have been left for 30 days wrapped in Teflon and in tin foil in the lab; (C) After the samples have been left for 4 days outdoors (cloudy weather); (D) After 45 minutes under the exhaust of a diesel car.

Figure 9(i), (ii) and (iii) show the decrease of NOx emissions between experiments (A) and (B), under all conditions of temperature and UV-irradiation. It confirms that NOx sources are depleted when asphalt is subjected to a flow of clean air, and subsequent cycles of temperature increases and UV-irradiations. Maximum emissions in (B) represent about 10% of the maximum emissions of (A) under all (T, UV) experimental conditions, with a more pronounced effect in the dark. It shows that NOx sources inside the material (*i.e.*, diffusion from the bulk to the surface of NOx precursors) are minor compared to sources coming from the environment. Interestingly, in experiment (C), a regeneration of the emissions is observed; leaving the samples outside, away from road traffic, seems sufficient to partly regenerate the NOx sources at 23°C in the dark, although steady-state values at 50°C in the dark and under UV are close to the values of (B), *i.e.* without regeneration. (D) shows that regeneration of NOx sources by a car's exhaust is very efficient with a diesel car. **Figure 9(i)** shows that the gas exhaust of a diesel car (D) has regenerated total NOx emissions much above their initial level at 23°C. At 50°C in the dark (**Figure 9(ii)**), regeneration is still efficient, but the maximum EF value is similar to the initial value, although with a higher NO/NO_2 ratio. At 50°C under UV (**Figure 9(iii)**), regeneration is observed, but to roughly one third of the initial NOx EF value.

Overall, these experiments point to the fact that asphalt itself is a relatively low NOx emitter, but is regenerated by everyday use with two types of sources; the first is clearly related to cars' exhaust, and the second is present in the environment, but not necessarily linked to traffic. It also confirms that the parent molecules releasing the NOx species detected are of different natures, as shown by their different behaviors with respect to thermal decomposition and photodecomposition leading to different NOx emission patterns in the dark and under UV-irradiation, and at the various temperatures investigated.

These results provide the basis to model NOx emissions by road asphalt on a daily basis, mimicking the temperature and UV-irradiation variations experienced by road surfaces during a day.

Regeneration of the sources of NOx, and therefore of the emissions, by the environment and by the traffic, depict a more accurate view of asphalt emission potential over long timescales, drawing a clearly non-zero base line for NO and NO_2 emissions. Old (LTA) asphalt therefore keeps emitting NOx all along its lifetime, allowing extension of the model to timescales longer than a day.

3.6. Mechanism Leading to NOx Emission by Asphalt Pavements

The main objective of this study is to evaluate the impact of NOx emissions of fresh and old asphalt pavements on urban air quality. Based on our experimental observations, *i.e.* emission trends of STA and LTA asphalt mixtures and regeneration experiments, several scenarios can be presented pertaining to the release of NOx. These scenarios should be viewed as new research directions aiming to explore NOx formation from this type of macroscopic surfaces.

To start with, the traffic-exposed old asphalt samples emit significantly higher amounts of NOx than fresh asphalt mixtures. The chemical aging of asphalt pavements by oxygen and other atmospheric radicals [Petersen and Glaser, 2011] certainly plays a dominant role on the behavior of the material, and on the way it interacts with pollutants.

A macroscopic surface like asphalt pavements provides multiple surface sites for adsorption or chemical transformation of pollutants. Asphalt pavements are a heterogeneous mixture of mineral aggregates (sand, gravel, crashed stones) held together by a bitumen binder. It is well established in the literature that NOx species and other organic and inorganic pollutants can be taken up or chemically transformed on heterogeneous mineral materials [Crowley *et al.*, 2010], [Romanias *et al.*, 2020], [Lasne *et al.*, 2018], [Lasne *et al.*, 2022]. Adsorption and chemical transformation of NOx on organic substrates have also been observed [Brigante *et al.*, 2008], [Cazoir *et al.*, 2014]. Therefore, in a first scenario we suggest that asphalt pavements are surfaces capable of adsorbing/taking up NOx species, either under ambient temperature conditions, or under higher temperatures during exposure to car exhausts. The adsorbed NOx can later desorb, releasing NO/NO_2 back to the gas phase. In this scenario, we consider that no chemical reaction /transformation affects NOx on the surface.

Alternatively, in a second scenario, NOx and other nitrogen-bearing pollutants can react with in asphalt pavements surfaces. These reactions can occur either via a Langmuir-Hinshelwood-type mechanism (*i.e.* NOx are first taken up and then react with organic or inorganic species present at the surface of asphalt), or via an Eley-Rideal mechanism (reaction of a molecule from the gas-phase with another species already adsorbed on the surface, which does not preclude uptake of the pollutant). In both cases, a chemical reaction occurs, that could lead to the formation of surface organic and inorganic nitrates, and of nitro-PAHs. It should be noted that these chemical reactions are anticipated to be more important on old asphalt mixtures, due to the slow oxidation of asphalt described by [Petersen and Glaser, 2011], that leads to the formation of alkoxy radicals (RO• surface species) which are extremely reactive to NO_2, and form organic nitrates [Atkinson, 2000]. Once formed, organic and inorganic nitrates can either be photolyzed by sunlight, or thermally decompose, releasing NOx species back to the gas phase.

We suggest that the second scenario, where the chemical transformation dominates, can explain totally our experimental findings. We also note that besides the RO• species, NOx could also react with closed shell molecules, like aromatic compounds and conjugated alkenes [Bernard *et al.*, 2013]. These reactions are generally slow [Bernard *et al.*, 2013], but could be sped up at high temperatures and high NOx concentrations (conditions relevant for car exhausts), and in the presence of catalysts. Heavy metals are naturally present in asphalt mixtures, or deposited on asphalt by car exhausts, tires, and brakes, and can act as photocatalysts [Khare *et al.*, 2020].

Finally, it should be noted that not only NOx, but other species can be formed during the exposure of asphalt pavements to traffic and atmospheric oxidants. For example, it is well established in the literature that nitrous acid (HONO) is formed in any NO_2 gas – surface interaction under humid conditions [Monge *et al.*, 2010], as observed in particular in urban areas [Lammel and Cape, 1996]. Once formed, HONO can also react and produce surface nitrates and NOx [Kim *et al.*, 2021]. To conclude, although several reaction pathways are presented in this section, dedicated studies need to be performed to clarify the reaction mechanism of NOx with macroscopic surfaces.

3.7. Model Simulations

3.7.1. Daily Profiles of NOx Emissions

To evaluate the impact of NOx emissions from asphalt pavements on urban air quality, the experimental observations are implemented in a city-scale model using Athens as a case study. Based on emission kinetics determined at different temperatures, we construct a daily profile that corresponds to atmospheric conditions of temperature (*i.e.*, air temperatures linked with asphalt surface temperatures based on our measurements, as indicated in **section 2.2**) for the reference period (September 2019). The experimental validation of NOx emission regeneration from traffic, as discussed in **section 3.5**, allows us to consider the same daily profile for the entire month of the simulation. **Table S4** provides the hourly data used in the model simulations, which are presented in the following section. Even if local materials and aging conditions are known to be somewhat different, we hypothesize, in a first approach, that the emissions composition of the old sample from Douai are representative of the emissions composition of old asphalt mixtures in Athens. Firstly, the asphalt pavements in Athens require a 40/50 penetration grade bitumen, which is similar to the bitumen grade of our samples (35/50). Moreover, the age of the old samples used in our study corresponds to the age of the road network in Athens (information provided by local authorities and newspapers, and also according to the decision Official Government Gazette 793 B΄, 31/12/81, of 1981), of about 30 years.

3.7.2. Simulation of NOx Emissions in Athens, Greece

Given the necessity to assess the impact of paved road emissions on urban atmospheric pollution, a modeling approach is devised to compare simulations with and without this emission source. The initial step is to assess the model's ability to reproduce the hourly concentration values in Athens. The evaluation is performed by comparing the model outputs to available measurements by the official regulatory monitoring network, and calculating the mean bias (MB), the root mean square error (RMSE) and the correlation coefficient (*r*) for NO_2 (see **Table S7**). Overall, the model tends to underestimate NO_2 concentrations, with mean MB and RMSE values of -12.8 μg m^{-3} and 7.3 μg m^{-3}, respectively (**Table S7**). The mean correlation among the hourly values of predictions and observations is 0.33, indicating a fair capability of the model to reproduce the hourly variation of NO_2. The main, systematic discrepancies in the intra-daily cycle are relevant to the timing of the day and nighttime peaks, which the model assigns later and earlier than observed, respectively. When correlating the daily values, the mean r reaches 0.6. With respect both to correlation and concentration differences, the model performs better at urban background areas than in the vicinity of other sources (vehicles or industry), which is expected due to the gridded (versus point) model (versus measured) outputs and the typical emission rates, compared to real-time emission activity. The model performance for this simulation study is consistent with previous high-resolution, model applications over the city of Athens [Athanasopoulou *et al.*, 2010], [Grivas *et al.*, 2020], [Ramacher *et al.*, 2021], [Gratsea *et al.*, 2021].

The mapping of surface mean monthly NO_2 concentrations (μg m^{-3}) is provided in **Figure 10**, together with the mean monthly *in situ* values measured at the stations. The hotspot areas are the

road network in the inner city (PER, PAT, GEO, ARI), and the greater areas around the main industrial and port activity of the domain. The resulting changes due to NOx emissions from asphalt surfaces are estimated through the normalized differences of the two model applications (with and without the emissions studied). Impacts above 5% to the total NO_2 mass during the hours of peak asphalt emissions (around midday) are shown by the blue isopleth in **Figure 10**, and can reach 20% at highway junctions. These areas extend around 100 km^2, while the fraction of road surfaces there does not exceed 10%, which is a typical value for the whole Athens urban center, according to Open Street Map data (https://planet.osm.org/). Nevertheless, the absolute hourly values of NO_2 concentrations that can be attributed to the specific emission source never exceed 0.7 μg m^{-3}, *i.e.*, ≈ 1% of measured levels at traffic stations, and ≈ 2.6% at background stations (see **Table S7**).

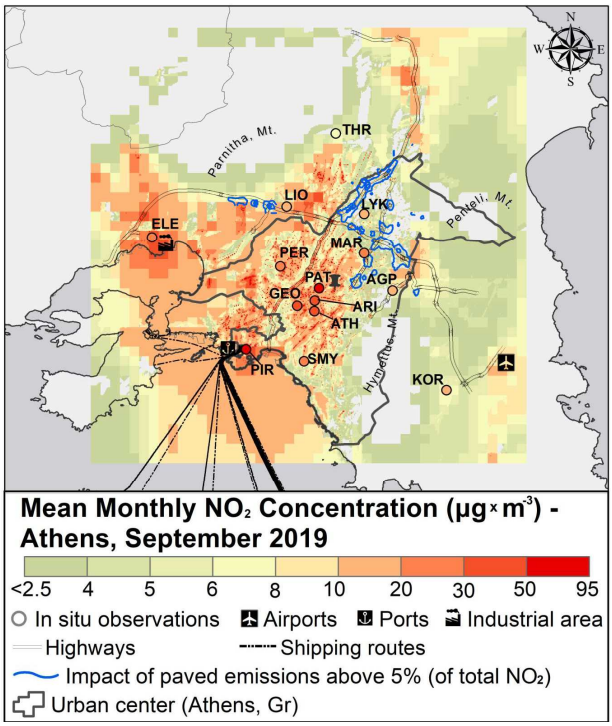

Figure 10: Mean monthly surface NO_2 concentrations (μg m^{-3}) over Athens (Greece), as modeled for September 2019. The measured values are shown in the color-coded circles. The blue isopleth corresponds to an impact of emissions from the paved surfaces higher than 5% of total NO_2 emissions.

On the other hand, Athens urban center has a relatively low coverage of paved road network (around 10% of total surface area), and high NOx emissions from traffic. Other European and American cities are characterized by higher asphalt-covered areas (possibly as high as 40% [Akbari *et al.*, 2003]), and generally lower NOx emissions from traffic. For example, in 2019, NOx emissions by road transport in Paris are almost half those of Athens, and in London, they are roughly five times weaker [https://www.ceip.at/the-emep-grid/gridded-emissions]. Therefore, NOx emissions by asphalt mixtures in Paris or London certainly represent a higher proportion of total NOx emissions. Furthermore, the reduction of air pollution from major sources, such as road traffic, are targeted by the European Green Deal and advocated for by the United Nations. It is therefore anticipated that NOx emissions from paved roads will gain a higher relative contribution in the future, and should not be overlooked.

4. Conclusions and Implications for Urban Air Quality

In the frame of this study, we combine laboratory experiments with city-scale modeling to evaluate the contribution of NOx emitted by asphalt pavements to urban air quality. Laboratory experiments evidence that atmospherically-aged asphalt pavements emit significantly more NOx than fresh asphalt mixtures. Even though the composition of both materials differ significantly in terms of nature and gradation of the aggregate, binder origin and content, and overall porosity, this work suggests that long-term exposure to traffic and atmospheric weathering are responsible for most of the observed differences. The impact of varying asphalt mixture compositions on emissions will be carefully studied in future work.

In order to gain a deeper understanding of the emission behavior of asphalt materials, we determine their emission characteristics as a function of time (emission kinetics), temperature, relative humidity, and light irradiation. Experiments are also performed to evaluate the atmospheric regeneration of the samples, and evidence that emissions of asphalt pavements are modified by air pollution, and especially by diesel car exhausts, showing that they should be viewed as a continuously renewed source of pollution.

To evaluate the impact of NOx emissions from asphalt pavements on urban air quality, model simulations are performed, using Athens as pilot city. The results of the model suggest that NOx emissions from traffic are by far the dominant source in the city center, with a contribution by asphalt pavements below 1% of total NOx emissions. Interestingly, outside the perimeter of the city center and at highway junctions, paved asphalt surfaces contribute to up to 20% of total NOx emissions. Therefore, NOx emissions from asphalt pavements should not be viewed as negligible, but their importance should rather be evaluated for each individual case. The development of scenarios modeling the impact of asphalt pavements on NOx and O_3 concentrations, and general urban air quality in the future, is necessary.

In addition, our results indicate that asphalt pavements are not the dominant missing source of NOx, that atmospheric models require to attenuate the difference with field observations (models underestimate by a factor of up to two NOx concentrations in urban environments). The emission efficiency of other macroscopic urban surfaces, (*e.g.*, building surfaces) on urban air quality, should be evaluated. The dry deposition of NOx, or related species, could be different in global urban environments modeled with all their complexity.

Lastly, this work raises the question of the parent molecules at the origin of NOx emissions; what is their nature, and how do they behave with respect to thermal decomposition and photo-decomposition to account for the observed NOx emissions? This is currently under investigation in our lab, together with a careful study of VOC emissions by asphalt, to give a more accurate picture of this already-observed phenomenon [Khare *et al.*, 2020]. Another perspective of this work is the study of the heterogeneous reactivity of pollutants, such as NOx and O_3, with the surface of asphalt, and the consequences on emissions by asphalt and on the structure and properties of the surface.

Acknowledgments

JL acknowledges funding from IMT Nord Europe through a post-doctoral fellowship in the frame of the IRAPAQ project, and a post-doctoral fellowship funded by ANR through the HygroPo-BBM project. TS acknowledges support from Institut National des Sciences de l'Univers of CNRS and LEFE (Les Enveloppes Fluides et l'Environnement) program through funding of the EmAPI project. EA, DK and AK acknowledge funding from the EU H2020 e-shape project (grant agreement 820852). The authors thank Dr Eric Hamonou for insightful discussions. The authors acknowledge ECCAD for archiving and distribution of the EMEP data. We are grateful to Mr. Jean-Etienne Régniez, Mr. Benjamin Choisel, and Mr. Benoit Varoqui (Mairie de Douai), for their assistance in the identification and characterization of the LTA asphalt mixture samples, and to Mr. Alexis Guilloteau (IMT Nord Europe) for granting access to the data of the weather station.

References

Akbari, H.; Rose, L.S.; Taha, H. Analyzing the land cover of an urban environment using high-resolution orthophotos. *Landsc. Urban Plann.* **63**, 1 (2003)

Alam, M.S.; Crilley, L.R.; Lee, J.D.; Kramer, L.J.; Pfrang, C.; Vázquez-Móreno, M.; Ródenas, M.; Muñoz, A.; Bloss, W.J. Interference from alkenes in chemiluminescent NOx measurements. *Atmos. Meas. Tech.* **13**, 5977 (2020)

Athanasopoulou, E.; Tombrou, M.; Russell, A.G.; Karanasiou, A.; Eleftheriadis, K.; Dandou, A. Implementation of road and soil dust emission parameterizations in the aerosol model CAMx: Applications over the greater Athens urban area affected by natural sources. *J. Geophys. Res.* **115**, D17301 (2010)

Atkinson, R. Atmospheric chemistry of VOCs and NOx. *Atmos. Environ.* **34**, 2063 (2000)

Barnard, J. C.; Chapman, E. G.; Fast, J. D.; Schmelzer, J. R.; Slusser, J. R.; Shetter, R. E. An evaluation of the FAST-J photolysis algorithm for predicting nitrogen dioxide photolysis rates under clear and cloudy sky conditions. *Atmos. Environ.* **38**, 3393 (2004)

Bernard, F.; Cazanau, M.; Mu, Y.; Wang, X.; Daële, V.; Chen, J.; Mellouki, A. Reaction of NO_2 with selected conjugated alkenes. *J. Phys. Chem. A* **117**, 14132 (2013)

Bohn, B.; Rohrer, F.; Brauers, T.; Wahner, A. Actinometric measurements of NO_2 photolysis frequencies in the atmosphere simulation chamber SAPHIR. *Atmos. Chem. Phys.* **5**, 493 (2005)

Borinelli, J.B.; Blom, J.; Portillo-Estrada, M.; Kara De Maeijer, P.; Van den bergh, W.; Vuye, C. VOC emission analysis of bitumen using proton-transfer reaction time-of-flight mass spectrometry. *Materials* **13**, Article number: 3659 (2020)

Brigante, M.; Cazoir, D.; D'Anna, B.; George, C.; Donaldson, D.J. Photoenhanced uptake of NO_2 by pyrene solid films. *J. Phys. Chem. A* **112**, 39 (2008)

Caron, F.; Guichard, R.; Robert, L.; Verriele, M.; Thevenet, F. Behaviour of individual VOCs in indoor environments: How ventilation affects emission from materials. *Atmos. Environ.* **243**, 117713 (2020)

Cavallari, J.M.; Osborn, L.V.; Snawder, J.E.; Kriech, A.J.; Olsen, L.D.; Herrick, R.F.; McClean, M.D. Predictors of airborne exposures to polycyclic aromatic compounds and total organic matter among hot-mix asphalt paving workers and influence of work conditions and practices. *Ann. Occup. Hyg.* **56**, 138 (2012a)

Cavallari, J.M.; Zwack, L.M.; Lange, C.R.; Herrick, R.F.; McClean, M.D. Temperature-dependent emission concentrations of polycyclic aromatic hydrocarbons in paving and built-up roofing asphalts. *Ann. Occup. Hyg.* **56**, 148 (2012b)

Cazoir, D. Brigante, M.; Ammar, R.; D'Anna, B.; George, C. Heterogeneous photochemistry of gaseous NO_2 on solid fluoranthene films: A source of gaseous nitrous acid (HONO) in the urban environment. *J. Photoch. Photobio. A* **273**, 23 (2014)

Crowley, J.N.; Ammann, M.; Cox, R.A.; Hynes, R.G.; Jenkin, R.E.; Mellouki, A.; Rossi, M.J.; Troe, J.; Wallington, T.J. Evaluated kinetic and photochemical data for atmospheric chemistry: Volume V – heterogeneous reactions on solid substrates. *Atmos. Chem. Phys.* **10**, 9059 (2010)

Espinoza, J.; Medina, C.; Calabi-Floody, A.; Sánchez-Alonso, E.; Valdés, G.; Quiroz, A. Evaluation of reductions in fume emissions (VOCs and SVOCs) from warm mix asphalt incorporating natural zeolite and reclaimed asphalt pavement for sustainable pavements. *Sustainability* **12**, 9546 (2020)

Fameli, K.M.; Assimakopoulos, V.D. Development of a road transport emission inventory for Greece and the Greater Athens Area: Effects of important parameters. *Sci. Total Environ.* **505**, 770 (2015)

Finlayson-Pitts, B.J.; Pitts Jr., J.N. Atmospheric Chemistry of Tropospheric Ozone Formation: Scientific and Regulatory Implications. *Air & Waste* **43**, 1091 (1993)

Gasthauer, E.; Mazé, M.; Marchand, J.P.; Amouroux, J. Characterization of asphalt fume composition by GC/MS and effect of temperature. *Fuel* **87**, 1428 (2008)

Gratsea, M.; Athanasopoulou, E.; Kakouri, A.; Richter, A.; Seyler, A.; Gerasopoulos, E. Five years of spatially resolved ground-based MAX-DOAS measurements of nitrogen dioxide in the urban area of Athens: Synergies with in situ measurements and model simulations. *Atmosphere* **12**, 1634 (2021)

Grivas, G.; Athanasopoulou, E.; Kakouri, A.; Bailey, J.; Liakakou, E.; Stavroulas, I.; Kalkavouras, P.; Bougiatioti, A.; Kaskaoutis, D.G.; Ramonet, M.; Mihalopoulos, N.; Gerasopoulos, E. Integrating in situ measurements and city scale modelling to assess the COVID–19 lockdown effects on emissions and air quality in Athens, Greece. *Atmosphere* **11**, 1174 (2020)

Health Effects Institute, State of Global Air 2020. *Special Report*. Boston, MA: Health Effects Institute (2020)

Higashiyama, H.; Sano, M.; Nakanishi, F.; Takahashi, O.; Tsukuma, S. Field measurements of road surface temperature of several asphalt pavements with temperature rise reducing function. *Case Stud. Constr. Mater.* **4**, 73 (2016)

Hofko, B.; Porot, L.; Falchetto Cannone, A.; Poulikakos, L.; Huber, L.; Lu, X.; Mollenhauer, K.; Grothe, H. FTIR spectral analysis of bituminous binders: reproducibility and impact of ageing temperature. *Mater. Struct.* **51**, Article number: 45 (2018)

Karl, M.; Walker, S.-E.; Solberg, S.; Ramacher, M.O.P. The Eulerian urban dispersion model EPISODE – Part 2, Extensions to the source dispersion and photochemistry for EPISODE - CityChem v1.2 and its application to the city of Hamburg. *Geosci. Model Dev.* **12**, 3357 (2019)

Khare, P.; Machesky, J.; Soto, R.; He, M.; Presto, A.A.; Gentner, D.R. Asphalt-related emissions are a major missing nontraditional source of secondary organic aerosol precursors. *Sci. Adv.* **6**, eabb9785 (2020)

Kim, Y.; Wu, Y.; Roustan, Y. Multi-scale modeling of urban air pollution: development and application of a Street-in-Grid model (v1.0) by coupling MUNICH (v1.0) and Polair3D (v1.8.1). *Geosci. Model Dev.* **11**, 611 (2018)

Kim, D.; Kim, J.; Lee, M.; Ahn, J.Y.; Lee, G. Assessment of Daytime HONO Emission Source from Asphalt Surface to Urban Air. *Appl. Sci.* **11**, 1930 (2021)

Kuik, F.; Kerschbaumer, A.; Lauer, A.; Lupascu, A.; von Schneidemesser, E.; Butler, T.M. Top–down quantification of NOx emissions from traffic in an urban urea using a high-resolution regional atmospheric chemistry model. *Atmos. Chem. Phys.* **18**, 8203 (2018)

Lammel, G.; Cape, J.N. Nitrous acid and nitrite in the atmosphere. *Chem. Soc. Rev.* **25**, 361 (1996)

Lasne, J.; Romanias, M.N.; Thevenet, F. Ozone uptake by clay dusts under environmental conditions. *ACS Earth Space Chem.* **2**, 904 (2018)

Lasne, J.; Urupina, D.; Maters, E.; Delmelle, P.; Romanias, M.N.; Thevenet, F. Photo-enhanced uptake of SO_2 on Icelandic volcanic dusts. *Environ. Sci.: Atmos.* **2**, 375 (2022)

Lelieveld, J.; Pozzer, A.; Pöschl, U.; Fnais, M.; Haines, A.; Münzel, T. Loss of life expectancy from air pollution compared to other risk factors: a worldwide perspective. *Cardiovasc. Res.* **116**, 1910 (2020)

Lesueur, D. The colloidal structure of bitumen: Consequences on the rheology and on the mechanisms of bitumen modification. *Adv. Colloid. Interfac.* **145**, 42 (2009)

Li, D.; Liao, W.; Rigden, A.J.; Liu, X.; Wang, D.; Malyshev, S.; Shevliakova, E. Urban heat island: Aerodynamics or imperviousness? *Sci. Adv.* **5**, eaau4299 (2019)

Monge, M.E.; D'Anna, B.; Mazri, L.; Giroir-Fendler, A.; Ammann, M.; Donaldson, D.J.; George, C. Light changes the atmospheric reactivity of soot. *P. Natl. Acad. Sci. USA* **107**, 6605 (2010)

Nilsson, P.T.; Bergendorf, U.; Tinnerberg, H.; Nordin, E.; Gustavsson, M.; Strandberg, B.; Albin, M.; Gudmundsson, A. Emissions into the air from bitumen and rubber bitumen—Implications for asphalt workers' exposure. *Ann. Work Expo. Heal.* **62**, 828 (2018)

Oikonomakis, E.; Aksoyoglu, S.; Ciarelli, G.; Baltensperger, U.; Prévôt, A.S.H. Low modeled ozone production suggests underestimation of precursor emissions (especially NOx) in Europe. *Atmos. Chem. Phys.* **18**, 2175 (2018)

Parison, S.; Hendel, M.; Grados, A.; Royon, L. Analysis of the heat budget of standard, cool and watered pavements under lab heat-wave conditions. *Energ. Buildings* **228**, 110455 (2020)

Petersen, J.C.; Glaser, R. Asphalt oxidation mechanisms and the role of oxidation products on age hardening revisited. *Road Mater. Pavement* **12**, 795 (2011)

Preiss, A.; Koch, A.W.; Kock, H.; Elend, M.; Raabe, M.; Pohlmann, G. Collection, validation and generation of bitumen fumes for inhalation studies in rats part 1: Workplace samples and validation criteria. *Ann. Occup. Hyg.* **50**, 789 (2006)

Ramacher, M.O.P.; Kakouri, A.; Speyer, O.; Feldner, J.; Karl, M.; Timmermans, R.; Denier van der Gon, H.; Kuenen, J.; Gerasopoulos, E.; Athanasopoulou, E. The UrbEm hybrid method to derive high-resolution emissions for city-scale air quality modeling. *Atmosphere* **12**, 1404 (2021)

Reimann, S.; Wegener, R.; Claude, A.; Sauvage, S. Updated Measurement Guideline for NOx and VOCs. *ACTRIS Deliverable* **D3.17** (2018).
https://www.actris.eu/sites/default/files/Documents/ACTRIS-2/Deliverables/WP3_D3.17_M42.pdf
(retrieved 2022-09-21)

Romanias, M.N.; Ren, Y.; Grosselin, B.; Daële, V.; Mellouki, A.; Dagsson-Waldhauserova, P.; Thevenet, F. Reactive uptake of NO2 on volcanic particles: A possible source of HONO in the atmosphere, *J. Env. Sci.* **95**, 155 (2020)

Sillman, S. The relation between ozone, NOx and hydrocarbons in urban and polluted rural environments. *Atmos. Environ.* **33**, 1821 (1999)

Solatifar, N.; Abbasghorbani, M.; Kavussi, A.; Sivilevičius, H. Prediction of depth temperature of asphalt layers in hot climate areas. *J. Civ. Eng. Manag.* **24**, 516 (2018)

Topaloglou, C.; Kazadzis, S.; Bais, A. F.; Blumthaler, M.; Schallhart, B.; Balis, D. NO2 and HCHO photolysis frequencies from irradiance measurements in Thessaloniki, Greece. *Atmos. Chem. Phys.* **5**, 1645 (2005)

Toraldo, E.; Mariani, E.; Alberti, S.; Crispino, M. Experimental investigation into the thermal behavior of wearing courses for road pavements due to environmental conditions. *Constr. Build. Mater.* **98**, 846 (2015)

United Nations, Department of Economic and Social Affairs, Population Division. World Urbanization Prospects: The 2018 Revision (ST/ESA/SER.A/420), New-York: United Nations (2019)

Villegas-Villegas, R.E.; Baldi-Sevilla, A.; Aguiar-Moya, J.P.; Loria-Salazar, L. Analysis of asphalt oxidation by means of accelerated testing and environmental conditions. *Transport Res. Rec.* **2672**, 244 (2018)

World Health Organization International Agency for Research on Cancer, Diesel and Gasoline Engine Exhausts and Some Nitroarenes. *IARC Monographs on the Evaluation of Carcinogenic Risks to Humans* **46** (1989)

World Health Organization International Agency for Research on Cancer, Bitumen and bitumen emissions, and some S- and N-heterocyclic polycyclic aromatic hydrocarbons. *IARC Monographs on the Evaluation of Carcinogenic Risks to Humans* **103** (2013)